

Breaking and trapping Cooper pairs by Rydberg-molecule spectroscopy in atomic Fermi superfluids

Chih-Chun Chien,^{1,2,*} S. I. Mistakidis,^{1,3} and H. R. Sadeghpour¹

¹*ITAMP, Center for Astrophysics | Harvard & Smithsonian, Cambridge, USA*

²*Department of Physics, University of California, Merced, CA, USA*

³*Department of Physics, Missouri University of Science and Technology, Rolla, MO, USA*

We propose a spectroscopic probe of the breaking and localization of Cooper pairs in an atomic Fermi superfluid interacting with a Rydberg impurity. This is achieved by monitoring the formation of diatomic and triatomic ultralong-range molecular species in the superfluid across the Bardeen–Cooper–Schrieffer (BCS)-Bose Einstein condensation (BEC) crossover. The triatomic Rydberg molecule in the BEC regime heralds the trapping of a tightly-bound Cooper pair, reminiscent of pion capture in nuclear matter, while the breaking of a Cooper pair on the BCS side by a diatomic Rydberg molecule is evocative of binary-star tidal disruption by a black hole. Spectroscopy of the Fermi superfluid and Rydberg molecules allows for an estimation of the Cooper-pair size while the Rydberg molecule binding energies discern many-body pairing effects.

Rydberg atom-based systems have emerged as leading platforms for demonstrating many-body correlations [1], quantum simulations [2–4], quantum error corrections [5], and quantum optics [6]. When the excited electron scatters from a nearby ground-state atom, under certain conditions, ultralong-range molecular bonds can form [7–9]. Such long-range Rydberg molecules have been realized [10–14], see also the reviews [15, 16]. Interesting aspects of many-body physics, such as the formation of Bose and Fermi polarons, quantum statistics of gases exhibiting bunching and anti-bunching, with Rydberg molecules have also been reported [17–21]. These studies exploit the large energy separations between the vibrational energies and the underlying primitive excitations in a quantum gas.

In a different context, two-component fermions with attractive interactions form Cooper pairs and exhibit the Bardeen-Cooper-Schrieffer (BCS) to Bose-Einstein condensation (BEC) crossover pioneered by the experiments with ultracold Fermi gases [22–24] (see also [25–27]). Here, we show that by creating ultralong-range molecules with a Rydberg impurity in a background sea of Cooper pairs, it is possible to a) break the pairs on the BCS side and b) locally trap a Cooper pair on the BEC side. The former bears analogies with the breaking of a binary-star pair by a tidal disruption event into a black hole [28, 29], while the latter is reminiscent of the capture of pions (quark-antiquark pairs) in hydrogen [30, 31], deuterium [32], and helium [33].

Rydberg molecules in Fermi superfluids offer a tabletop laboratory to simulate analogues in stellar and nuclear settings [34]. Through radio-frequency (rf) spectroscopy of the superfluid pairing gap [35, 36] or Rydberg spectroscopy of the molecular lines [17, 19], one may probe the reaction of the superfluid to tackle topical problems in condensed matter physics, such as the Cooper-pair size and pairing energies [37].

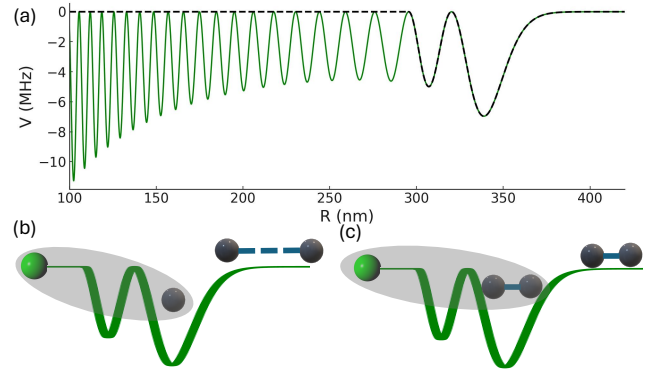


FIG. 1. (a) A typical Rydberg potential (solid line) and the outer double-well approximation (dashed line). The formation of (b) a diatomic Rydberg molecule with a fermion from a broken Cooper pair and (c) a triatomic Rydberg molecule with a Cooper pair. The green (black) spheres represent the Rydberg atoms (fermions in the superfluid). The Cooper pairs are visualized by two black spheres connected by a dashed or solid line. The grey ellipsoids mark the Rydberg molecules.

A typical Rydberg potential is illustrated in Fig. 1 with heteronuclear Rydberg molecules formed in Fermi superfluids. These molecules are (1) diatomic between the impurity and a fermion from a broken Cooper pair and (2) triatomic, or “a Cooper pair in a molecule” since a Cooper pair is trapped by the Rydberg potential. To our knowledge, the latter type of Rydberg molecules has not been discussed in the literature, and they are different from the trimer Rydberg molecules emanating from two weakly interacting bosons individually trapped by a bosonic Rydberg atom that have been realized [38] and theoretically studied [39, 40]. Therefore, the Rydberg molecules in Fermi superfluids exploit the interplay and competition between two molecule-formation mechanisms, one between the fermions to bind a Cooper pair and the other among the Rydberg and its neighboring atoms to create a Rydberg molecule.

* cchien5@ucmerced.edu

Leveraging the Bogoliubov-de Gennes (BdG) formalism [41, 42] suitable for studying inhomogeneous effects in Fermi superfluids, we extract the low-lying bound states of the composite Rydberg-Fermi superfluid system. By increasing the Cooper-pair strength, distinct local reactions of the pairing gap to the Rydberg potential will occur: Breaking (trapping) of a weak (strong) Cooper pair leads to a local suppression (enhancement) of the gap function. We identify the formation of diatomic and triatomic Rydberg molecules along with their binding energies, which are raised by the many-body pairing effect when compared to those in a noninteracting gas. In contrast to previous studies [43] with impurities carrying onsite potentials in Fermi superfluids, the Rydberg potential has its furthest well about hundreds of nanometers away from the core with controllable width and depth, thereby giving rise to rich structures of Rydberg molecules.

Rydberg atoms in a Fermi superfluid.— We consider few Rydberg atoms immersed in a two-component, spin- and mass-balanced Fermi superfluid with contact pairing interactions. Experimentally, this setup can be emulated, for instance, by bosonic ^{87}Rb Rydberg atoms and two hyperfine states of ^{86}Rb for the Fermi superfluid. However, our results equally hold for other Rydberg atom-Fermi superfluid systems. For simplicity, the Rydberg atoms are assumed to be immobile in real space and noninteracting with each other. A quasi one-dimensional (1D) geometry [44] creating a cigar-shaped cloud similarly to Refs. [24, 45] is considered. It supports the off-diagonal long-range order of the superfluid while freezing out the transverse degrees-of-freedom.

The many-body Hamiltonian of the composite system within the BCS-Leggett theory reads

$$\mathcal{H} = \mathcal{H}_{BCS} + \sum_{\sigma} \int dx V_{Ryd}(x) \psi_{\sigma}^{\dagger}(x) \psi_{\sigma}(x) d^{\dagger} d, \quad (1)$$

where $\mathcal{H}_{BCS} = \int dx \left[\sum_{\sigma} \psi_{\sigma}^{\dagger}(x) h_{\sigma}(x) \psi_{\sigma}(x) + (\Delta(x) \psi_{\uparrow}^{\dagger}(x) \psi_{\downarrow}^{\dagger}(x) + h.c.) \right]$ [25, 46]. The fermion operator acting on the $\sigma = \uparrow, \downarrow$ component of mass m is ψ_{σ} , and $h_{\sigma}(x) = -\frac{\hbar^2}{2m} \nabla^2 + V_{ext}(x) - \mu_{\sigma}$ denotes the single-particle Hamiltonian with $V_{ext}(x)$ summarizing the total external confinement and influence. The order parameter of the s -wave Fermi superfluid is the gap function

$$\Delta(x) = -U \langle \psi_{\downarrow}(x) \psi_{\uparrow}(x) \rangle. \quad (2)$$

The effective coupling $U < 0$ is related to the 1D scattering length a_{1D} [47] via $U = -\frac{2\hbar^2}{ma_{1D}}$, tunable by Feshbach resonance [25], and $\langle \dots \rangle$ designates the ground-state expectation value at $T = 0$. The BCS-BEC crossover occurs when the chemical potential (here $\mu_{\uparrow} = \mu_{\downarrow} \equiv \mu$) crosses zero [27] where the minimum of the quasiparticle spectrum shifts to zero momentum.

Importantly, the second contribution in Eq. (1) models the Rydberg atom - fermion interaction [20], with d (d^{\dagger})

being the annihilation (creation) operator of a Rydberg atom. The ultralong-range Born-Oppenheimer potential between a Rydberg atom and a ground-state fermionic atom is given by $V_{Ryd}(x) = \frac{2\pi\hbar^2 a_e}{m_e} |\psi_e(x)|^2$ [7]. Here, a_e denotes the scattering length between the Rydberg electron with mass m_e and a fermionic atom, and x measures the distance from the Rydberg impurity to the fermionic atom. The atomic Rydberg wave function, $\psi_e(x)$, is calculated with effective valence potentials [48]. In the vicinity of a Rydberg atom, we replace $d^{\dagger} d$ by $\langle d^{\dagger} d \rangle = 1$ and hence $V_{Ryd}(x)$ acts as an external potential for the Fermi superfluid. In what follows, it will be implicitly combined with $V_{ext}(x)$ in h_{σ} . Moreover, the Fermi energy $E_f = \hbar^2 k_f^2 / (2m)$ and wavevector $k_f = \pi n / 2$, of a noninteracting 1D two-component Fermi gas with the same total particle number $N = \int n(x) dx$ as the superfluid, serve as the energy and inverse-length units. For example, $g = -U k_f / E_f$ is the dimensionless coupling constant of pairing between the fermions.

BdG formalism.— To reveal the impact of the Rydberg atoms on the Fermi superfluid, we inspect the composite system as the superfluid undergoes the BCS-BEC crossover. Specifically, \mathcal{H} can be diagonalized by the BdG transformation [42, 49]: $\psi_{\uparrow}(x) = \sum_{\tilde{n}} [u_{\uparrow}^{\tilde{n}1}(x) \gamma_{\tilde{n}1} - v_{\uparrow}^{\tilde{n}2*}(x) \gamma_{\tilde{n}2}]$ and $\psi_{\downarrow}(x) = \sum_{\tilde{n}} [u_{\downarrow}^{\tilde{n}2}(x) \gamma_{\tilde{n}2} + v_{\downarrow}^{\tilde{n}1*}(x) \gamma_{\tilde{n}1}]$. The quasiparticle wave functions $u_{\sigma}^{\tilde{n}j}$ and $v_{\sigma}^{\tilde{n}j}$ with $j = 1, 2$ are to be determined, and they satisfy $\int dx (|u_{\sigma}^{\tilde{n}j}|^2 + |v_{\sigma}^{\tilde{n}j}|^2) = 1$. The BdG equation for the composite system considered here can be block-diagonalized into [42]

$$\begin{pmatrix} h_{\uparrow}(x) & \Delta(x) \\ \Delta^*(x) & -h_{\downarrow}^*(x) \end{pmatrix} \begin{pmatrix} u_{\uparrow}^{\tilde{n}j}(x) \\ v_{\downarrow}^{\tilde{n}j}(x) \end{pmatrix} = E_{\tilde{n}j} \begin{pmatrix} u_{\uparrow}^{\tilde{n}j}(x) \\ v_{\downarrow}^{\tilde{n}j}(x) \end{pmatrix}. \quad (3)$$

Moreover, the BdG equation has a discrete symmetry connecting the positive and negative energy states, so we drop the indices 1, 2 and \uparrow, \downarrow from the quasi-particle wave functions. For the ground state, the gap function Eq. (2) then becomes $\Delta(x) = -U \sum_{\tilde{n}}' u_{\uparrow}^{\tilde{n}}(x) v_{\downarrow}^{\tilde{n}*}(x)$ and the total fermion density $n(x) = \sum_{\sigma} n_{\sigma}(x) = 2 \sum_{\tilde{n}}' |v_{\tilde{n}}(x)|^2$ with $n_{\sigma}(x) = \langle \psi_{\sigma}^{\dagger}(x) \psi_{\sigma}(x) \rangle$. Here $\sum_{\tilde{n}w}'$ denotes summation over the positive-energy states. We discretize the space and implement an iterative method [42, 50] to solve the BdG equation (see SM [51] for details).

Discussion.— The interaction between a Rydberg impurity and nearby fermions is determined by the Rydberg potential shown in Fig. 1. To account for the impenetrable core of the Rydberg atom, the system is further embedded in a 1D box of size L with the Rydberg atom at $x = 0$ and appropriately adjusting the relevant energy and length scales, see also SM [51]. The gap function and density of a representative BCS (BEC) Fermi superfluid with $\mu > 0$ ($\mu < 0$) subjected to the Rydberg potential are depicted in the left (right) panels of Fig. 2. While the density profiles on both BCS and BEC sides show peaks evidencing the bound states due to the attractive Rydberg potential, the most prominent contrast is the enhancement (suppression) of the gap function around

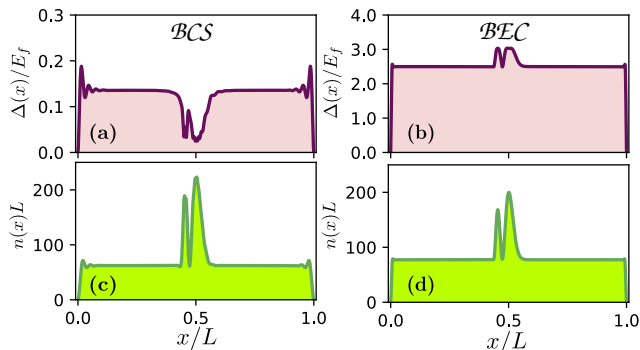


FIG. 2. Gap function Δ (top panels) and density (bottom panels) of a Fermi superfluid in the BCS regime with $g = 0.9$, $\mu = 0.40E_f$ (left panels) and the BEC regime where $g = 3.8$ and $\mu = -0.06E_f$ (right panels) under the same Rydberg potential. Reduced (enhanced) undulations of $\Delta(x)$ near the wells of the Rydberg potential are evident in the BCS (BEC) regime.

the minima of the Rydberg potential in the BEC (BCS) regime. The decoupling of the gap function and density of a Fermi superfluid on the BCS side has been discussed in vortex structures [52, 53], and here the Rydberg potential provides another concrete example. We mention the oscillatory boundary effects on the BCS side due to its fermionic excitations, which is explained in the SM [51].

The bound-state wave functions $v_n(x)$ of the Rydberg potential in the BCS and BEC regimes are presented in Fig. 3, see the SM [51] for all bound-state wave functions u_n and v_n . It is evident that each well may host a series of bound states when the depth of the Rydberg potential is enough to compete with the pairing in the Fermi superfluid. Thus, there is a competition between the intercomponent fermion attraction to maintain the Cooper pairs and the attraction among the Rydberg atom and the fermions to form molecules. The bound-state energies in the BCS regime are clearly separated, and each bound state consists of a single fermion. This implies that the resulting diatomic Rydberg molecules originate from individual fermions due to broken Cooper pairs.

The bound states in the BEC regime shown in Fig. 3(b) are more complex. Indeed, focusing on the furthest well, the first two bound states are clearly separated in energy, indicating that they correspond to diatomic Rydberg molecules. However, the subsequent two higher vibrational bound states in the same well are energetically adjacent with almost identical wave functions. Together with the enhanced gap function shown in Fig. 2, the twin bound states suggest the presence of a locally trapped Cooper pair. Therefore, the furthest well hosts a triatomic Rydberg molecule as an excited vibrational state in the BEC regime due to the combination of the strong Cooper pairing and the Rydberg potential being capable of trapping the Cooper pair. There is also a pair of bound states with almost identical binding energies and wave functions localized in the secondary well illus-

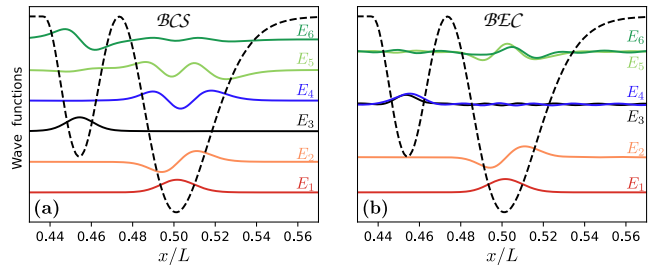


FIG. 3. Bound vibrational wave functions $v_n(x)$ of the Rydberg potential (dashed lines) depicted in Fig. 1 offset according to their energies E_n . The Fermi superfluid is in the (a) BCS regime with $g = 0.9$ and $\mu = 0.4E_f$ and (b) BEC regime with $g = 3.8$ and $\mu = -0.06E_f$. On the BEC side, there are two sets of nearly degenerate vibrational states localized respectively in the inner and outer wells, heralding the formation of triatomic heteronuclear Rydberg molecules.

trated in Fig. 3(b). These are again evident of the creation of another triatomic Rydberg molecule. Therefore, the double-well approximate Rydberg potential depicted in Fig. 1 is able to host both diatomic and triatomic Rydberg molecules.

The Cooper-pair size may be estimated by the BCS coherence length [46]

$$\xi \approx \frac{\hbar v_f}{\Delta}, \quad (4)$$

where v_f is the Fermi velocity. For the Rydberg potential and box confinement used here, the width of the furthest (secondary) well is about $0.06L$ ($0.03L$). The Cooper-pair size of the selected BCS (BEC) case of Fig. 2 is $\xi/L \approx 0.07$ ($\xi/L \approx 0.003$) since $\Delta/E_f \approx 0.14$ and $k_f L \approx 111$ ($\Delta/E_f \approx 2.5$ and $k_f L \approx 131$). Hence, the Cooper pairs on the BCS side cannot be accommodated within the Rydberg-potential wells. In this context, only a fermion from a broken Cooper pair is captured, forming a diatomic molecule. In contrast, the Cooper pairs of the BEC case may fit into the Rydberg potential, which is deep enough to either break a Cooper pair or trap it to form a diatomic or a triatomic Rydberg molecule.

For a typical cold-atom cloud with density $n \approx 10^{13} \text{ cm}^{-3}$ [25], $E_f \approx 1 \text{ kHz}$ for Rb atoms, the depth of the Rydberg potential in Fig. 1 reaches the order of MHz. The pairing gap is roughly of the order of E_f as shown in Fig. 2, which can be orders of magnitude smaller than the depth of the Rydberg potential even on the BEC side. The Rydberg molecule lifetime is typically about $10\text{-}100 \mu\text{s}$ [15], while the timescale in a Fermi gas is governed by \hbar/E_f ($\sim 1 \text{ ms}$ here). Therefore, the above treatment of quasi-equilibrium Fermi superfluids in the presence of Rydberg molecules is reasonable. Meanwhile, a shallow Rydberg potential discussed in the SM [51] with similar orders of magnitude of the pairing gap and potential depth is shown to also form diatomic and triatomic Rydberg molecules.

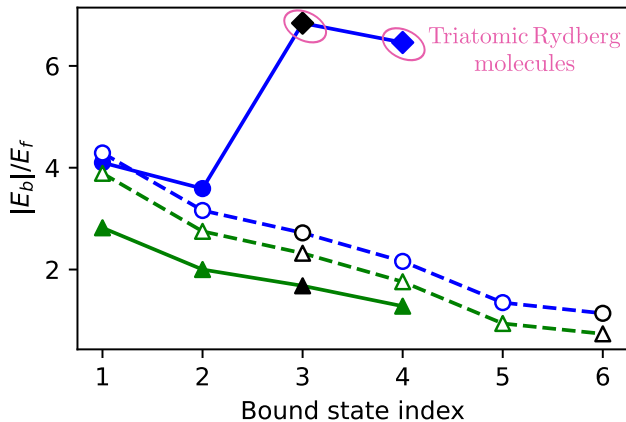


FIG. 4. Normalized binding energies from the BdG equation (circles and diamonds) and the Schrödinger equation (triangles) with the Rydberg potential of Fig. 1. Solid and hollow circles and triangles (diamonds) denote diatomic (triatomic) Rydberg molecules. Dashed (solid) lines connect the data on the BCS (BEC) side with $g = 0.9$ and $\mu = 0.4E_f$ ($g = 3.8$ and $\mu = -0.06E_f$). Blue and green (black) symbols denote the bound states in the outer (inner) well of the Rydberg potential. Each triatomic Rydberg molecule binds a Cooper pair.

The respective binding energies (normalized by E_f) obtained from the BdG equation with the Rydberg potential of Fig. 1 are illustrated in Fig. 4. The first two lowest-energy bound states in both BCS and BEC regimes have comparable binding energies since they correspond to diatomic Rydberg molecules consisting of the Rydberg atom and a broken-pair fermion. However, the binding energies of the higher vibrational bound states in the BCS and BEC regimes deviate more significantly because the triatomic Rydberg molecules in the BEC possess relatively larger binding energies within the trapped Cooper pairs.

We remark that the relation between the diatomic and triatomic Rydberg molecules in Fermi superfluids is more complex than that in a BEC [17] due to spin statistics and many-body effects. Indeed, adding an identical boson to a Rydberg dimer leads to a triatomic molecule with twice the diatomic binding energy. However, this does not hold for fermions due to the Pauli exclusion. Specifically, the formation of diatomic and triatomic Rydberg molecules in a Fermi superfluid competes with the binding of Cooper pairs. As such, the many-body contribution of breaking or trapping a Cooper pair plays a decisive role in creating Rydberg molecules, as it becomes apparent by the BdG calculation shown in Fig. 4.

To discern many-body from single-particle effects in the Rydberg molecule formation, we also evaluate the binding energies of diatomic Rydberg molecules with the Schrödinger equation $(h_\sigma + V_{Ryd})\psi_\sigma = E_n^S\psi_\sigma$, with h_σ from \mathcal{H}_{BCS} ; see also SM [51] for the underlying bound states. The normalized single-particle binding energies are presented in Fig. 4. The many-body binding energies

obtained from the BdG equation are in general larger than the corresponding single-particle energies due to pairing effect. However, the binding energies in the BCS regime follow a similar trend with the single-particle energies, and their energy difference remains roughly constant as higher vibrational states are reached.

In contrast, the BdG binding energies on the BEC side exhibit larger deviations from their single-particle counterparts. For the diatomic Rydberg molecules, this is because the stronger pairing makes the Fermi superfluid on the BEC side with $\mu < 0$ quite different from a noninteracting gas. Based on the gap function shown in Fig. 2, the energy difference between the many-body and single-particle binding energies of the diatomic Rydberg molecules are of the same order as the pairing energy. Moreover, the emergence of the triatomic Rydberg molecules results in a substantial energy difference from the noninteracting counterpart due to the trapped Cooper pair, with its own binding energy.

Implications.— Spatially resolved rf spectroscopy of atomic Fermi superfluids [35, 36], following original attempts in Refs. [54, 55], map out the local pairing gap. As described in Fig. 2, this will determine the types of Rydberg molecules since the pairing is suppressed (enhanced) in the diatomic (triatomic) Rydberg molecule. Meanwhile, the Rydberg molecules in a Fermi superfluid may serve as a probe for the Cooper-pair size because triatomic Rydberg-molecule formation is only possible when the Cooper-pair size is smaller than the width of the Rydberg potential. Differentiating the diatomic and triatomic Rydberg molecules is also achievable by Rydberg-molecule line spectroscopy [17, 19] since the binding energy of a triatomic Rydberg molecule is substantially larger than that of a diatomic one, as shown in Fig. 4. The Rydberg impurity-Fermi superfluid system features several tunable parameters, including the depth, width, and location of the Rydberg potential, determined by the Rydberg excitation [15, 16], and the pairing strength and particle density of the Fermi superfluid (see, e.g., Refs. [25, 46]).

Furthermore, the quasi-1D setup has several advantages. First, the Rydberg lifetime in a lattice is found to be longer for reduced dimensions [56]. If the enhancement also holds in the continuum, it facilitates Rydberg-molecule formation in 1D as there is on average one fermion within the Rydberg orbit, in the cases studied here. Second, the rotational excitations of Rydberg molecules will be less relevant in 1D, significantly simplifying the bound-state spectrum. Moreover, the 1D geometry eases i) the comparison between the Cooper-pair size and the Rydberg potential width, ii) the identification of diatomic or triatomic Rydberg molecules, and iii) the characterization of the Rydberg molecules, e.g., from the density and pairing gap profiles.

So far, the Rydberg atoms are assumed to be of different isotopes or species from the Fermi superfluid. Alternatively, if some of the fermions within the superfluid are excited into Rydberg atoms, forming homonuclear Ryd-

berg molecules, this results in a reduced effective pairing gap $\Delta' = \Delta - g_l n_R$, see also the discussion in the SM [51]. Here, g_l is the coupling constant for exciting the fermions to Rydberg atoms. Once the excited Rydberg atoms are present, however, the corresponding bound states can be extracted through the BdG formalism. Therefore, dimer or trimer Rydberg molecules are expected via Rydberg excitations stemming from the Fermi superfluid although the reduced effective pairing gap will favor dimer Rydberg molecules.

Finally, we note that Rydberg molecules are different from the Cooper-pair splitting in superconductor heterostructures [57–62]. In this case, the proximity effect is utilized by dynamically sending a Cooper pair, as an excited state with spin entanglement or momentum correlation, to two separate non-superconducting regions in real space. In contrast, the fermion bound in a diatomic Rydberg molecule no longer retains the pairing correlation, while the tightly-bound Cooper pair in a triatomic Rydberg molecule localizes in real space. Along the same lines, there are subtle differences between the Rydberg molecules in Fermi superfluids and the binary tidal disruption event and pion matter. For instance, binding in binary stars (pion matter) stems from gravity (Coulomb interactions), whereas in Rydberg molecules, it is traced back to the electron-atom scattering.

Summary and outlook.— The bound states of Fermi superfluids in a Rydberg-impurity potential testify to the formation of Rydberg molecules. The tunable fermion pairing gives rise to diatomic Rydberg molecules from broken Cooper pairs and triatomic Rydberg molecules from tightly-bound Cooper pairs, exhibiting different features of the gap function due to their distinctive nature. The detection of the triatomic Rydberg molecules may reveal information about the Cooper-pair size while the bound-state energies reflect pairing effects. With the rapid developments of Rydberg physics and Fermi gases, realizations of Rydberg molecules in Fermi superfluids will provide an elegant example of interfacing few- and many-body physics in a unified platform. Furthermore, going beyond the Leggett-BCS theory [25, 46] of the superfluid ground state, pre-formed Cooper pairs at finite temperatures correct the superfluid transition temperature and lead to the pseudo-gap effect away from the BCS regime [63, 64]. Incorporating pairing-fluctuation theories developed for homogeneous systems [27, 65–67] into the BdG formalism remains a challenge, and finite-temperature physics of Rydberg molecules awaits future research.

Acknowledgements.— C. C. C. was partly supported by the NSF (No. PHY-2310656). Support for ITAMP by the NSF is also acknowledged.

-
- [1] A. Browaeys and T. Lahaye, Many-body physics with individually controlled Rydberg atoms, *Nature Physics* **16**, 132 (2020).
- [2] M. Saffman, T. G. Walker, and K. Mølmer, Quantum information with Rydberg atoms, *Rev. Mod. Phys.* **82**, 2313 (2010).
- [3] C. S. Adams, J. D. Pritchard, and J. P. Shaffer, Rydberg atom quantum technologies, *Journal of Physics B: Atomic, Molecular and Optical Physics* **53**, 012002 (2019).
- [4] X. Wu, X. Liang, Y. Tian, F. Yang, C. Chen, Y.-C. Liu, M. K. Tey, and L. You, A concise review of Rydberg atom based quantum computation and quantum simulation, *Chinese Physics B* **30**, 020305 (2021).
- [5] D. Bluvstein, S. J. Evered, A. A. Geim, S. H. Li, H. Zhou, T. Manovitz, S. Ebadi, M. Cain, M. Kalinowski, D. Hangleiter, J. P. Bonilla Ataides, N. Maskara, I. Cong, X. Gao, P. Sales Rodriguez, T. Karolyshyn, G. Semeghini, M. J. Gullans, M. Greiner, V. Vuletić, and M. D. Lukin, Logical quantum processor based on reconfigurable atom arrays, *Nature* **626**, 58 (2024).
- [6] X. Q. Shao, S. L. Shi-Lei Su, L. Li, R. Nath, J. H. Wu, and W. Li, Rydberg superatoms: An artificial quantum system for quantum information processing and quantum optics (2024), arXiv: 2404.05330.
- [7] C. H. Greene, A. S. Dickinson, and H. R. Sadeghpour, Creation of Polar and Nonpolar Ultra-Long-Range Rydberg Molecules, *Phys. Rev. Lett.* **85**, 2458 (2000).
- [8] M. I. Chibisov, A. A. Khuskivadze, and I. I. Fabrikant, Energies and dipole moments of long-range molecular Rydberg states, *J. Phys. B: At. Mol. Opt. Phys.* **35**, L193 (2002).
- [9] E. L. Hamilton, C. H. Greene, and H. R. Sadeghpour, Shape-resonance-induced long-range molecular Rydberg states, *J. Phys. B: At. Mol. Opt. Phys.* **35**, L199 (2002).
- [10] V. Bendkowsky, B. Butscher, J. Nipper, J. P. Shaffer, R. Löw, and T. Pfau, Observation of ultralong-range rydberg molecules, *Nature* **458**, 1005 (2009).
- [11] T. Niederprüm, O. Thomas, T. Eichert, C. Lippe, J. Pérez-Ríos, C. H. Greene, and H. Ott, Observation of pendular butterfly Rydberg molecules, *Nature Communications* **7**, 12820 (2016).
- [12] M. Althön, M. Exner, R. Blättner, and H. Ott, Exploring the vibrational series of pure trilobite Rydberg molecules, *Nature Communications* **14**, 8108 (2023).
- [13] D. Booth, S. T. Rittenhouse, J. Yang, H. R. Sadeghpour, and J. P. Shaffer, Production of trilobite Rydberg molecule dimers with kilo-Debye permanent electric dipole moments, *Science* **348**, 99 (2015), <https://www.science.org/doi/pdf/10.1126/science.1260722>.
- [14] J. D. Whalen, S. K. Kanungo, Y. Lu, S. Yoshida, J. Burgdörfer, F. B. Dunning, and T. C. Killian, Heteronuclear rydberg molecules, *Phys. Rev. A* **101**, 060701 (2020).
- [15] J. P. Shaffer, S. T. Rittenhouse, and H. R. Sadeghpour, Ultracold Rydberg molecules, *Nature Communications* **9**, 1965 (2018).
- [16] F. H. Christian Fey and P. Schmelcher, Ultralong-range Rydberg molecules, *Molecular Physics* **118**, e1679401 (2020).
- [17] F. Camargo, R. Schmidt, J. D. Whalen, R. Ding, G. Woehl, S. Yoshida, J. Burgdörfer, F. B. Dunning,

- H. R. Sadeghpour, E. Demler, and T. C. Killian, Creation of Rydberg Polarons in a Bose Gas, *Phys. Rev. Lett.* **120**, 083401 (2018).
- [18] R. Schmidt, H. R. Sadeghpour, and E. Demler, Mesoscopic Rydberg Impurity in an Atomic Quantum Gas, *Phys. Rev. Lett.* **116**, 105302 (2016).
- [19] R. Schmidt, J. D. Whalen, R. Ding, F. Camargo, G. Woehl, S. Yoshida, J. Burgdörfer, F. B. Dunning, E. Demler, H. R. Sadeghpour, and T. C. Killian, Theory of excitation of Rydberg polarons in an atomic quantum gas, *Phys. Rev. A* **97**, 022707 (2018).
- [20] J. Sous, H. R. Sadeghpour, T. C. Killian, E. Demler, and R. Schmidt, Rydberg impurity in a Fermi gas: Quantum statistics and rotational blockade, *Phys. Rev. Res.* **2**, 023021 (2020).
- [21] A. A. T. Durst and M. T. Eiles, Phenomenology of a Rydberg impurity in an ideal Bose Einstein condensate (2024), arXiv: 2404.03980.
- [22] M. Greiner, C. A. Regal, and D. S. Jin, Emergence of a molecular Bose–Einstein condensate from a Fermi gas, *Nature* **426**, 537 (2003).
- [23] M. W. Zwierlein, C. A. Stan, C. H. Schunck, S. M. F. Raupach, A. J. Kerman, and W. Ketterle, Condensation of Pairs of Fermionic Atoms near a Feshbach Resonance, *Phys. Rev. Lett.* **92**, 120403 (2004).
- [24] M. Bartenstein, A. Altmeyer, S. Riedl, S. Jochim, C. Chin, J. H. Denschlag, and R. Grimm, Collective Excitations of a Degenerate Gas at the BEC-BCS Crossover, *Phys. Rev. Lett.* **92**, 203201 (2004).
- [25] C. J. Pethick and H. Smith, *Bose–Einstein Condensation in Dilute Gases*, 2nd ed. (Cambridge University Press, 2008).
- [26] M. Ueda, *Fundamentals and New Frontiers of Bose–Einstein Condensation* (World Scientific, Singapore, 2010) <https://www.worldscientific.com/doi/pdf/10.1142/7216>.
- [27] W. Zwerger, ed., *The BCS-BEC Crossover and the Unitary Fermi Gas* (Springer Berlin, Heidelberg, 2012).
- [28] J. G. Hills, Hyper-velocity and tidal stars from binaries disrupted by a massive galactic black hole, *Nature* **331**, 687 (1988).
- [29] B. C. Bromley, S. J. Kenyon, M. J. Geller, and W. R. Brown, Binary disruption by massive black holes: Hypervelocity stars, s stars, and tidal disruption events, *The Astrophysical Journal Letters* **749**, L42 (2012).
- [30] D. Gotta, F. Amaro, D. F. Anagnostopoulos, S. Biri, D. S. Covita, H. Gorke, A. Gruber, M. Hennebach, A. Hirtl, T. Ishiwatari, P. Indelicato, T. Jensen, E.-O. L. Bigot, J. Marton, M. Nekipelov, J. M. F. dos Santos, S. Schlessler, P. Schmid, L. M. Simons, T. Strauch, M. Trassinelli, J. F. C. A. Veloso, and J. Zmeskal, Pionic hydrogen, in *Precision Physics of Simple Atoms and Molecules*, edited by S. G. Karshenboim (Springer Berlin Heidelberg, Berlin, Heidelberg, 2008) pp. 165–186.
- [31] A. Hirtl, D. F. Anagnostopoulos, D. S. Covita, H. Fuhrmann, H. Gorke, D. Gotta, A. Gruber, M. Hennebach, P. Indelicato, T. S. Jensen, E.-O. L. Bigot, Y.-W. Liu, V. E. Markushin, J. Marton, M. Nekipelov, J. M. F. d. Santos, L. M. Simons, T. Strauch, M. Trassinelli, J. F. C. A. Veloso, and J. Zmeskal, Redetermination of the strong-interaction width in pionic hydrogen, *The European Phys. J. A* **57**, 70 (2021).
- [32] T. Strauch, F. D. Amaro, D. F. Anagnostopoulos, P. Bühler, D. S. Covita, H. Gorke, D. Gotta, A. Gruber, A. Hirtl, P. Indelicato, E.-O. Le Bigot, M. Nekipelov, J. M. F. dos Santos, P. Schmid, S. Schlessler, L. M. Simons, M. Trassinelli, J. F. C. A. Veloso, and J. Zmeskal, Pionic deuterium, *The European Phys. J. A* **47**, 88 (2011).
- [33] M. Hori, H. Aghai-Khozani, A. Sótér, A. Dax, and D. Barna, Recent results of laser spectroscopy experiments of pionic helium atoms at PSI, *SciPost Phys. Proc.* , 026 (2021).
- [34] J. S. Cohen, Capture of negative exotic particles by atoms, ions and molecules, *Rep. Progr. Phys.* **67**, 1769 (2004).
- [35] Y. Shin, C. H. Schunck, A. Schirotzek, and W. Ketterle, Tomographic rf spectroscopy of a trapped fermi gas at unitarity, *Phys. Rev. Lett.* **99**, 090403 (2007).
- [36] P. A. Murthy, M. Neidig, R. Klemt, L. Bayha, I. Boettcher, T. Enss, M. Holten, G. Zürn, P. M. Preiss, and S. Jochim, High-temperature pairing in a strongly interacting two-dimensional Fermi gas, *Science* **359**, 452 (2018), <https://www.science.org/doi/pdf/10.1126/science.aan5950>.
- [37] C. H. Schunck, Y.-i. Shin, A. Schirotzek, and W. Ketterle, Determination of the fermion pair size in a resonantly interacting superfluid, *Nature* **454**, 739 (2008).
- [38] V. Bendkowsky, B. Butscher, J. Nipper, J. B. Balewski, J. P. Shaffer, R. Löw, T. Pfau, W. Li, J. Stanojevic, T. Pohl, and J. M. Rost, Rydberg Trimers and Excited Dimers Bound by Internal Quantum Reflection, *Phys. Rev. Lett.* **105**, 163201 (2010).
- [39] I. C. H. Liu, J. Stanojevic, and J. M. Rost, Ultra-Long-Range Rydberg Trimers with a Repulsive Two-Body Interaction, *Phys. Rev. Lett.* **102**, 173001 (2009).
- [40] J. A. Fernandez, P. Schmelcher, and R. Gonzalez-Ferez, Ultralong-range triatomic Rydberg molecules in an electric field, *J. Phys. B: At. Mol. Opt. Phys.* **49**, 124002 (2016).
- [41] P. G. De Gennes, *Superconductivity of Metals and Alloys.*, 2nd ed., Advanced Books Classics (Chapman and Hall/CRC, Boulder, 2018).
- [42] J.-X. Zhu, *Bogoliubov-de Gennes Method and Its Applications*, 1st ed., Lecture Notes in Physics, 924 (Springer International Publishing, Cham, 2016).
- [43] H. Hu, L. Jiang, H. Pu, Y. Chen, and X.-J. Liu, Universal Impurity-Induced Bound State in Topological Superfluids, *Phys. Rev. Lett.* **110**, 020401 (2013).
- [44] S. Mistakidis, A. Volosniev, R. Barfknecht, T. Fogarty, T. Busch, A. Foerster, P. Schmelcher, and N. Zinner, Few-body bose gases in low dimensions—a laboratory for quantum dynamics, *Phys. Rep.* **1042**, 1 (2023), few-body Bose gases in low dimensions—A laboratory for quantum dynamics.
- [45] M. C. Revelle, J. A. Fry, B. A. Olsen, and R. G. Hulet, 1d to 3d Crossover of a Spin-Imbalanced Fermi Gas, *Phys. Rev. Lett.* **117**, 235301 (2016).
- [46] A. J. Leggett, *Quantum Liquids : Bose condensation and Cooper pairing in condensed-matter systems*, Oxford Graduate Texts (Oxford University Press, Oxford, UK, 2006).
- [47] M. Olshanii, Atomic Scattering in the Presence of an External Confinement and a Gas of Impenetrable Bosons, *Phys. Rev. Lett.* **81**, 938 (1998).
- [48] M. Marinescu, H. R. Sadeghpour, and A. Dalgarno, Dispersion coefficients for alkali-metal dimers, *Phys. Rev. A* **49**, 982 (1994).

- [49] N. Bogoliubov, On the theory of superfluidity, *J. Phys.* **11**, 23 (1947).
- [50] B. Parajuli and C.-C. Chien, Proximity effect and spatial Kibble-Zurek mechanism in atomic Fermi gases with inhomogeneous pairing interactions, *Phys. Rev. A* **107**, 063314 (2023).
- [51] See Supplemental Material for details on the BdG formalism, the impact of higher Rydberg excitations in the molecule formation, the effect of the Rydberg potential location, further information on the bound states, the formation of homonuclear Rydberg molecules and the creation of Rydberg molecules in a noninteracting gas.
- [52] C.-C. Chien, Q. Chen, Y. He, and K. Levin, Finite temperature effects in trapped Fermi gases with population imbalance, *Phys. Rev. A* **74**, 021602 (2006).
- [53] Y. He and C.-C. Chien, Vortex structure and spectrum of an atomic Fermi superfluid in a spherical bubble trap, *Phys. Rev. A* **108**, 053303 (2023).
- [54] J. Kinnunen, M. Rodríguez, and P. Törmä, Pairing Gap and In-Gap Excitations in Trapped Fermionic Superfluids, *Science* **305**, 1131 (2004), <https://www.science.org/doi/pdf/10.1126/science.1100782>.
- [55] A. Schirotzek, Y.-i. Shin, C. H. Schunck, and W. Ketterle, Determination of the Superfluid Gap in Atomic Fermi Gases by Quasiparticle Spectroscopy, *Phys. Rev. Lett.* **101**, 140403 (2008).
- [56] J. Zeiher, J.-y. Choi, A. Rubio-Abadal, T. Pohl, R. van Bijnen, I. Bloch, and C. Gross, Coherent Many-Body Spin Dynamics in a Long-Range Interacting Ising Chain, *Phys. Rev. X* **7**, 041063 (2017).
- [57] G. B. Lesovik, T. Martin, and G. Blatter, Electronic entanglement in the vicinity of a superconductor, *The European Phys. J. B - Condensed Matter and Complex Systems* **24**, 287 (2001).
- [58] P. Recher, E. V. Sukhorukov, and D. Loss, Andreev tunneling, coulomb blockade, and resonant transport of non-local spin-entangled electrons, *Phys. Rev. B* **63**, 165314 (2001).
- [59] L. Hofstetter, S. Csonka, J. Nygård, and C. Schönberger, Cooper pair splitter realized in a two-quantum-dot Y-junction, *Nature* **461**, 960 (2009).
- [60] A. Ranni, F. Brange, E. T. Mannila, C. Flindt, and V. F. Maisi, Real-time observation of Cooper pair splitting showing strong non-local correlations, *Nature Communications* **12**, 6358 (2021).
- [61] F. Brange, R. Baruah, and C. Flindt, Adiabatic Cooper pair splitter, *Phys. Rev. B* **109**, L081402 (2024).
- [62] J. Schindele, A. Baumgartner, and C. Schönberger, Near-Unity Cooper Pair Splitting Efficiency, *Phys. Rev. Lett.* **109**, 157002 (2012).
- [63] J. P. Gaebler, J. T. Stewart, T. E. Drake, D. S. Jin, A. Perali, P. Pieri, and G. C. Strinati, Observation of pseudogap behaviour in a strongly interacting Fermi gas, *Nature Phys.* **6**, 569 (2010).
- [64] X. Li, S. Wang, X. Luo, Y.-Y. Zhou, K. Xie, H.-C. Shen, Y.-Z. Nie, Q. Chen, H. Hu, Y.-A. Chen, X.-C. Yao, and J.-W. Pan, Observation and quantification of the pseudogap in unitary fermi gases, *Nature* **626**, 288 (2024).
- [65] K. Levin, Q. Chen, C.-C. Chien, and Y. He, Comparison of different pairing fluctuation approaches to BCS-BEC crossover, *Annals of Physics* **325**, 233 (2010).
- [66] M. Randeria and E. Taylor, Crossover from Bardeen-Cooper-Schrieffer to Bose-Einstein Condensation and the Unitary Fermi Gas, *Annual Review of Condensed Matter Physics* **5**, 209 (2014).
- [67] E. J. Mueller, Review of pseudogaps in strongly interacting Fermi gases, *Reports on Progress in Physics* **80**, 104401 (2017).

Supplemental Material: Breaking and trapping Cooper pairs by Rydberg-molecule spectroscopy in atomic Fermi superfluids

I. BOGOLIUBOV-DE GENNES CALCULATION

After diagonalization by the BdG transformation (see the main text), the many-body Hamiltonian takes the form $\mathcal{H} = \sum_{\bar{n}w} E_{\bar{n}w} \gamma_{\bar{n}w}^\dagger \gamma_{\bar{n}w} + E_g$. In this expression, $w = 1, 2$ represents the quasi-particle components, E_g is the ground-state energy, and $\sum_{\bar{n}w}$ denotes summation over the positive-energy states. The ground-state energy is $E_g = -\frac{|\Delta|^2}{U} + \sum_{\bar{n}, w} (\epsilon_{\bar{n}w} - E_{\bar{n}w})$ with $\epsilon_{\bar{n}w}$ being the non-interacting counterpart of the excitation energy $E_{\bar{n}w}$. The BdG equation has the symmetry $\begin{pmatrix} u_{\downarrow}^{\bar{n}2}(x) \\ v_{\uparrow}^{\bar{n}2}(x) \end{pmatrix} = \begin{pmatrix} v_{\downarrow}^{\bar{n}1*}(x) \\ -u_{\uparrow}^{\bar{n}1}(x) \end{pmatrix}$ with $E_{\bar{n}2} = -E_{\bar{n}1}$. The quasi-particle operators obey $\langle \gamma_{\bar{n}w}^\dagger \gamma_{\bar{m}v} \rangle = \delta_{\bar{n}\bar{m}} \delta_{wv} f(E_{\bar{n}w})$ and $\langle \gamma_{\bar{n}w} \gamma_{\bar{m}v} \rangle = \langle \gamma_{\bar{n}w}^\dagger \gamma_{\bar{m}v}^\dagger \rangle = 0$ with $f(E) = [e^{E/K_B T} + 1]^{-1}$ being the Fermi distribution function. At finite temperatures, the gap function becomes $\Delta(x) = -U \sum_{\bar{n}} u_{\uparrow}^{\bar{n}}(x) v_{\downarrow}^{\bar{n}*}(x) \tanh(E_{\bar{n}}/k_B T)$ and the total Fermi density $n(x) = \sum_{\sigma} n_{\sigma}(x) = n(x) = 2 \sum_{\bar{n}} |v_{\bar{n}}(x)|^2 (1 - f(E_{\bar{n}})) + |u_{\bar{n}}(x)|^2 f(E_{\bar{n}})$. We caution that a bound state with $E_n < 0$ contributes to the density via $|u_n|^2$. Due to the symmetry, it is equivalent to a $E_n > 0$ state contributing to the density via $|v_n|^2$.

In our numerical calculations, we consider a quasi-1D system in a 1D box of length L . We discretize the space $x/L = [0, 1]$ using n_x grid points $x_j = j\delta x$, where $\delta x = L/n_x$ and $j = 0, 1, 2, \dots, n_x - 1$. The BdG equation is also discretized by using the finite-difference method and becomes

$$\sum_j \begin{pmatrix} h_{ij} & \Delta_{ij} \\ \Delta_{ij}^* & -h_{ij} \end{pmatrix} \begin{pmatrix} u_j^{\bar{n}} \\ v_j^{\bar{n}} \end{pmatrix} = E_{\bar{n}} \begin{pmatrix} u_i^{\bar{n}} \\ v_i^{\bar{n}} \end{pmatrix}. \quad (\text{S1})$$

Here $\Delta_{ij} = \Delta_i \delta_{i,j}$ for s -wave pairing. The BdG Hamiltonian has the size of $2n_x \times 2n_x$ and we only take the positive energy eigenstates for the calculations of the gap function and density. For the ground state of the Fermi superfluid, the total density becomes

$$n(x) = 2 \sum_{\bar{n}} |v_{\bar{n}}(x)|^2. \quad (\text{S2})$$

The total fermion number is $N = N_{\uparrow} + N_{\downarrow} = \int_0^L n(x) dx$. The gap function is given by

$$\Delta(x) = -U \sum_{\bar{n}} u_{\bar{n}}(x) v_{\bar{n}}(x). \quad (\text{S3})$$

The Rydberg atom is placed at $x = 0$, where the wave functions should vanish due to the impenetrable core of the Rydberg atom. The box boundary at $x = L$ is chosen such that the wave functions return to the bulk values before encountering the wall at $x = L$. The box introduces an energy scale $E_0 = \hbar^2/(2mL^2)$, but we use the

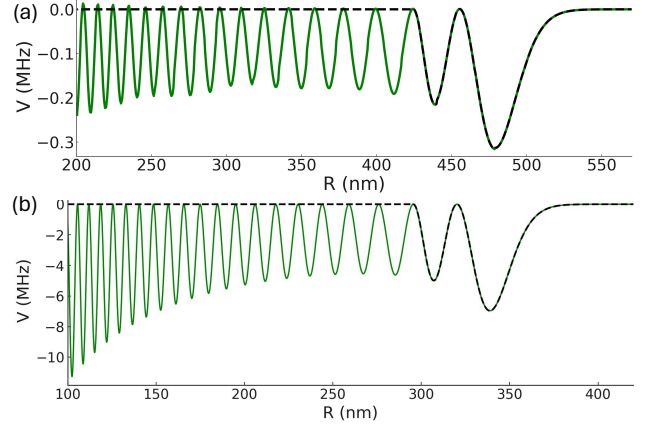


FIG. S1. Typical Rydberg potentials from (a) Sr(71S) state and (b) Rb(62S) Rydberg excitation. The solid (dashed) lines are the full potentials (outer double-well approximations).

intrinsic inverse-length and energy units k_f and E_f carried by the fermions. Numerically, we start with a trial $\Delta(r)$ and a given set of parameters (U, μ) in order to solve the BdG equation and thus obtain the eigenvalues and eigenstates of the Rydberg atom-Fermi superfluid system. The gap function is then assembled for the next iteration. The iteration stops when the convergence condition $(1/L) \int_0^L dx ||\Delta^{new}(x) - \Delta^{old}(x)||/E_0 < \epsilon$ is satisfied, where $\Delta^{new/old}(x)$ denote the gap functions between consecutive iterations. We have taken $\epsilon = 10^{-6}$ and 1000 grid points and checked that further adjustments of those values do not cause qualitative changes.

Let us also comment on the oscillatory boundary effects due to the box confinement on the BCS side in the profiles shown in Fig. 2 of the main text. The Fermi superfluid on the BCS side has relatively weak pairing. Therefore, when the boundary enforces the gap function and density to vanish, the fermions behave as noninteracting ones exhibiting an oscillatory behavior with length scale $1/k_f$. This is because noninteracting fermions form a Fermi sea and the perturbation of the system starts at the Fermi momentum, which then results in the aforementioned oscillations at the boundary. In contrast, the fermions form tightly bound pairs on the BEC side, which behave like composite bosons and no longer follow the Fermi statistics. On the BEC side, the composite bosons are repelled by the box boundaries, but they vanish smoothly without the oscillatory behavior. We emphasize that the box confinement is a simple choice to satisfy the impenetrability condition of the Rydberg atom, and the focus should be on the Rydberg-molecule formation due to the Rydberg potential instead of the boundary effects due to the choice of the confinement.

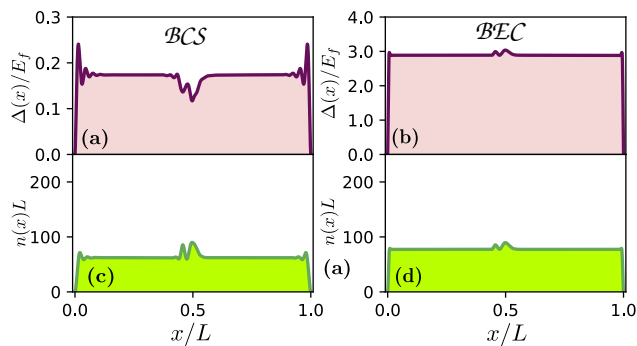


FIG. S2. Profiles of the gap function (top row) and density (bottom row) of a Fermi superfluid in the BCS regime with $g = 1.0$ and $\mu = 0.52E_f$ (left column) and BEC regime with $g = 4.1$ and $\mu = -0.07E_f$ (right column). The Rydberg potential stems from the Sr(71S) Rydberg state and its furthest dip is located at $R_0 = L/2$.

II. HIGHER RYDBERG EXCITATION

Upon considering a higher Rydberg excitation results in a shallower Rydberg potential. As a paradigmatic example, here, we assume the Sr(71S) Rydberg state in a Fermi superfluid. Since the most relevant part of the Rydberg potential corresponds to the two dips furthest away from its core, we smooth out the highly oscillatory potential located close to the core. A comparison of the Rydberg potentials from the Rb(62S) state and that from the Sr(71S) state is given in Fig. S1, along with the approximation concerning their two furthest potential wells used in the BdG calculations. When the two potentials are placed in a 1D box with the furthest dips at its center and the length and energy scales properly scaled, as explained below, the potential from the Rb(62S) state is about ten times deeper. The two Rydberg potentials thus allow us to contrast the characteristics of the emergent Rydberg molecules in Fermi superfluids.

Placing the approximate double-well Rydberg potential in a 1D box accounts for the impenetrable core of the Rydberg atom and provides a consistent comparison when different Rydberg states are used. We extract the distance R_0 from the core to the furthest dip and its depth V_0 of the Rydberg potential. For a selected Rydberg atom and its state, R_0 and V_0 are related. For example, $R_0 = 480$ nm and $V_0 = 0.32$ MHz for the Sr(71S) Rydberg state in a ^{87}Sr Fermi superfluid. The aspect ratio of the Rydberg potential is fixed by introducing the energy scale $E_R = \hbar^2/(2mR_0^2)$ and obtaining the ratio V_0/E_R . By setting $R_0 = \alpha L$ with $0 < \alpha < 1$, the furthest dip is located at αL inside the box. This also fixes the energy relation $E_R = E_0/\alpha^2$, from which the Rydberg potential can be expressed in terms of the corresponding k_f and E_f .

By squeezing the Rydberg potential towards the left of the box with a smaller α , the effective depth of the potential increases, but the widths of the wells decrease. As

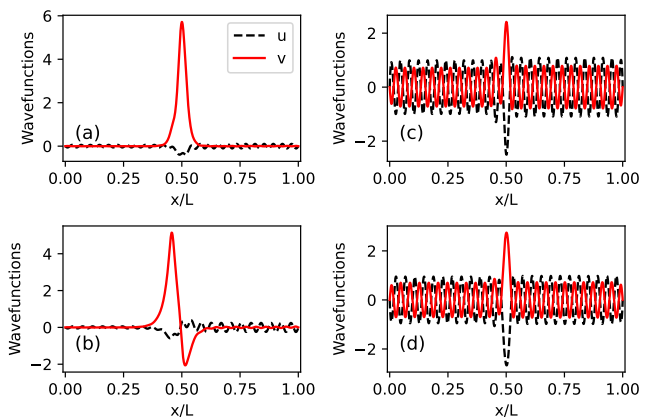


FIG. S3. Bound-state wave functions of a Fermi superfluid under the Sr(71S) Rydberg potential in the BCS regime with $g = 1.0$ and $\mu = 0.52E_f$ (left panels) and BEC regime with $g = 4.1$ and $\mu = -0.07E_f$ (right panels). The bound states on the BCS side are of broken-pair nature while the two on the BEC side are from a trapped Cooper pair. The furthest well of the Rydberg potential is at $R_0 = L/2$.

shown below, the case with $\alpha = 1/4$ exhibits similar behavior on the BCS and BEC sides as those where $\alpha = 1/2$ being presented here. This indicates that the number of bound states is determined by a combination of the potential width and depth. Thus, a simple rescaling of the Rydberg potential inside the box does not lead to further qualitative changes. In the following, we will place the furthest dip of the Rydberg potential at $x = L/2$ and scale its depth accordingly.

The left column of Figure S2 shows the profiles of the gap function and the density for a selected case in the BCS regime with $\mu > 0$ and the potential taken from the Sr(71S) Rydberg state. The presence of the Rydberg potential causes a dip in the gap function, which implies a suppression of pairing, and a peak in the density, indicating that unpaired fermions accumulate.

Before analyzing the energy spectrum and wave functions of the BCS case, we show in the right column of Fig. S2 the profiles of the gap function and density of a Fermi superfluid on the BEC side with $\mu < 0$ under the same Rydberg potential. In stark contrast to the BCS case, the gap function features a peak at the location of the Rydberg potential. The same behavior is evident on the density profile. Thus, the pairing is enhanced inside the Rydberg potential when the Fermi superfluid is BEC-like. The enhancement of pairing also suggests that Cooper pairs are trapped by the Rydberg atom.

To explain the contrast between the BCS and BEC cases, we analyze the eigen-functions obtained from the BdG equation, see Fig. S3. Since the symmetry of the BdG equation guarantees that every positive energy eigen-state is accompanied by a negative-energy state, a bound state of a particle is also accompanied by a bound state of a hole having the opposite energy sign. For this reason, we examine the profiles of the eigen-functions and

identify the bound states with localized patterns in the potential wells. For the BCS and BEC cases presented in Fig. S2, most of the eigen-states exhibit oscillatory behavior in the box (not shown for brevity). Nevertheless, we identify particular states featuring localization at the dips of the Rydberg potential. The left column of Fig. S3 depicts the two energetically lowest localized states on the BCS side that can be identified with this Rydberg potential. From the number of nodes inside the Rydberg potential, one may classify them as the first and second bound states localized in the rightmost potential well.

The binding energies of these two bound states on the BCS regime are not adjacent to each other, implying that they are between a fermion and the Rydberg atom as only individual fermionic states well separated in energy are involved. This behavior suggests that the composite object refers to a diatomic Rydberg molecule. The suppression of the gap function on the BCS side can also be understood in terms of the formation of the Rydberg molecules, which breaks a Cooper pair when a fermion falls into the Rydberg potential. Meanwhile, the fermionic atom from a broken Cooper pair in the Rydberg molecule causes a bump in the local density, reminiscent to the occupation of the vortex core by unpaired fermions [52, 53].

For the BEC case demonstrated in the right column of Fig. S2, there are also two bound states localized in the Rydberg potential. However, the two localized states have adjacent energies and similar wave functions, as can be seen in the right column of Fig. S3. Therefore, two fermions are constituting the first bound state in the Rydberg potential in the BEC regime. This is a direct indication that a tightly-bound Cooper pair falls into the Rydberg potential and forms a three-body bound state, or a Rydberg molecule with a Rydberg atom and a Cooper pair. Therefore, a triatomic Rydberg molecule forms in the BEC case presented here. For the Sr(71S) Rydberg potential, however, the depth is too shallow to host additional bound states.

We also estimate the Cooper-pair size using Eq. (4) in the main text and compare it with the width of the Rydberg potential. For the Sr(71S) Rydberg state, the width of the furthest well is about $0.04L$ after placing it at $x/L = 0.5$ of the box. For the BCS case selected above, $\Delta/E_f \approx 0.18$ and $k_f L \approx 98$, which lead to $\xi/L \approx 0.06$. Meanwhile, $\Delta/E_f \approx 2.9$ and $k_f L \approx 121$ for the shallow-BEC case selected above, so $\xi/L \approx 0.003$. Therefore, the width of the Cooper pairs on the BCS (BEC) side is larger (smaller) than the width of the primary Rydberg-potential well. This also corroborates that a fermion from a broken Cooper pair is trapped by the Rydberg potential to form a diatomic Rydberg molecule when the Fermi superfluid is on the BCS side. In contrast, the relatively shallow Rydberg potential traps a Cooper pair on the BEC side in its primary well, forming “a Cooper pair in a molecule”. Moreover, as compared to the relatively deep Rydberg-potential discussed in the main text, the

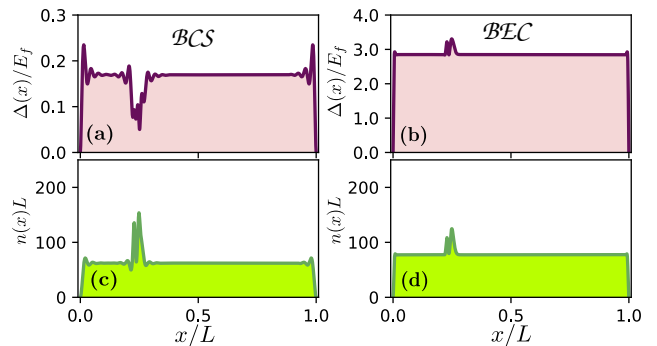


FIG. S4. Profiles of the gap function (top row) and density (bottom row) of a Fermi superfluid in the BCS regime with $g = 1.0$ and $\mu = 0.52E_f$ (left column) and the BEC regime with $g = 4.1$ and $\mu = -0.07E_f$ (right column). The potential is created by the Sr(71S) Rydberg state and has its furthest dip at $R_0 = L/4$.

secondary well of the shallower Rydberg potential presented here does not support bound states.

III. ADJUSTING THE LOCATION OF THE RYDBERG POTENTIAL

Here we take the potential of the Sr(71S) Rydberg state but set $R_0 = L/4$, i.e., $\alpha = 1/4$. Using this scaling, the depth of the potential increases due to the relatively smaller R_0 , but the width of the potential reduces. Fig. S4 presents the profiles of the gap function and the density on the BCS side and BEC side, respectively, under the Sr(71S) Rydberg potential. Similar to the $\alpha = 1/2$ case, the pairing is suppressed on the BCS side but is enhanced on the BEC side. Meanwhile, the density exhibits a peak on both BCS and BEC sides, signaling the emergence of bound states.

The left column of Fig. S5 illustrates the localized eigenstates extracted from the BdG equation corresponding to the setup on the BCS side depicted in Fig. S4. It becomes apparent that there are again two bound states with clearly separated binding energies. By examining the nodes of the wave functions, we can infer that they are the first and second bound states of the Rydberg potential. Therefore, the Rydberg atom breaks a Cooper pair and traps a fermionic atom to form a diatomic Rydberg molecule.

In contrast, when the Fermi superfluid is in the BEC regime, the right column of Fig. S5 shows the localized eigenstates corresponding to the right column of Fig. S4. There are two bound states with adjacent binding energies and similar wave functions, indicating that a Cooper pair has been trapped by the Rydberg potential. Therefore, the triatomic Rydberg molecule in this case consists of the Rydberg atom and a Cooper pair trapped by its potential. Squeezing the Rydberg potential within the box increases its depth and reduces its width, but it is

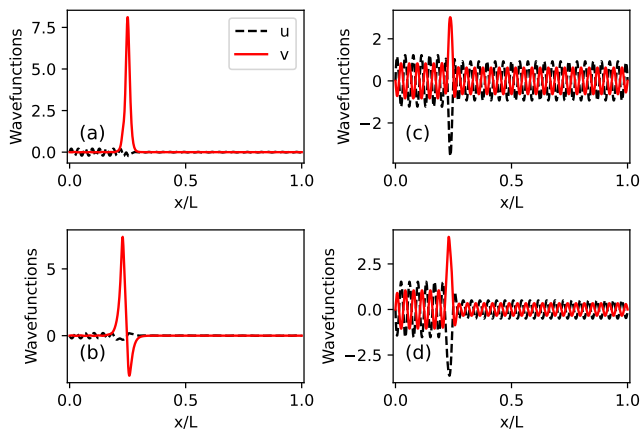


FIG. S5. Bound-state profiles of a Fermi superfluid under the Sr(71S) Rydberg potential in the BCS regime with $g = 1.0$ and $\mu = 0.52E_f$ (left column) and the BEC regime with $g = 4.1$ and $\mu = -0.07E_f$ (right column). The rightmost well of the Rydberg potential is located at $R_0 = L/4$.

still not sufficient to break a tightly bound Cooper pair in the shallow BEC regime in this case.

IV. DETAILS OF BOUND STATES

The bound state wave functions $v_n(x)$ of the Rydberg potential are summarized in Fig. 3 of the main text. Here, for reasons of completeness, we provide the full bound-state wave functions u_n and v_n of the Fermi superfluid under the Rydberg potential shown in Fig. 1 of the main text. Specifically, Fig. S6 presents the localized eigenstates in the Rydberg potential which are extracted from the BdG analysis in the BCS case. Panels (a) to (f) depict, in a hierarchical order, the lowest-energy bound state to the highest-energy one. Since the bound-state energies are well separated and each bound state corresponds to a fermion, the bound states of Fig. S6 are indicative of diatomic molecule formation.

Fig. S7 shows the bound states calculated from the BdG equation in the BEC regime utilizing the same Rydberg potential. As can be seen, there are two energetically distinct bound states localized in the furthest well [Fig. S7(a), (b)] followed by two almost identical lowest-energy bound states localized in the secondary well [Fig. S7(c), (d)] and another two almost identical bound states localized in the furthest well [Fig. S7(e), (f)]. Each pair of the twin bound states corresponds to a Cooper pair trapped by the Rydberg potential. However, the secondary well on the left traps a Cooper pair into its lowest bound state [Fig. S7(c), (d)], while the furthest well traps a Cooper pair as its third vibrational state [Fig. S7(e), (f)].

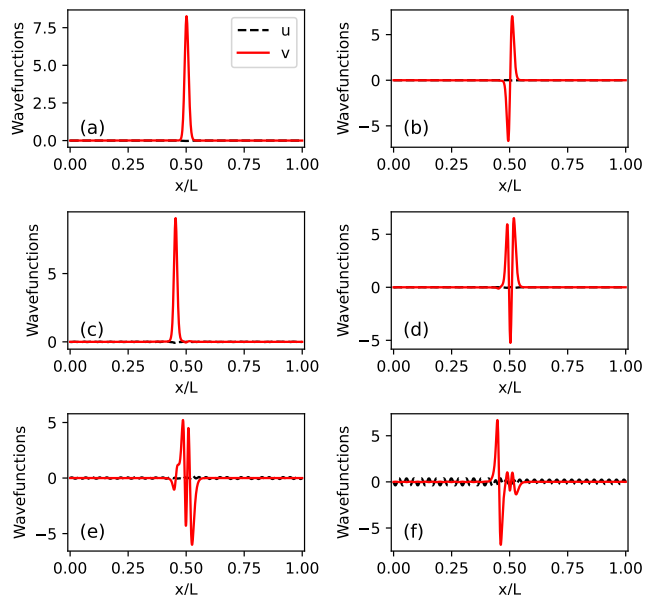


FIG. S6. Bound-state profiles of a Fermi superfluid in the BCS regime with $g = 0.9$ and $\mu = 0.40E_f$ with the Rb(62S) Rydberg potential. The magnitude of binding energies decreases monotonically from (a) to (f). Here (a), (b), (d), (e) are the energetically lowest first four bound states in the right well, while (c) and (f) refer to the first two in the left well. All states here are from broken-pair fermions.

V. EXCITING RYDBERG ATOMS WITHIN THE FERMION SUPERFLUID

Here, instead of introducing bosonic isotopes or atoms of different species as Rydberg impurities in an atomic Fermi superfluid, we consider the alternative process of exciting the atoms of the Fermi superfluid to produce Rydberg atoms. In this case, our description should be modified in order to account for the excitation of Rydberg atoms from the Fermi superfluid. This process is modelled by means of considering the additional Hamiltonian term $H_{ex} = g_l \int dx (d^\dagger \tilde{\psi}^\dagger(x) \psi_\downarrow(x) \psi_\uparrow(x) + h.c.)$ which, in practice, converts a Cooper pair into a Rydberg atom and an unpaired fermion. In this expression, $\tilde{\psi}^\dagger$ is the creation operator of a fermion from the broken Cooper pair but without excitation to the Rydberg state, d^\dagger refers to the creation operator of a Rydberg atom, and g_l is the coupling constant for exciting the Rydberg atoms. Since a Cooper pair needs to be broken to create a Rydberg atom in this case, g_l is expected to be larger than the pairing coupling constant U .

If the Rydberg-atom density n_R from the broken Cooper pairs satisfies $n_R R_0^3 \ll 1$, with R_0 denoting the range of the Rydberg potential, we may approximate $\langle d^\dagger \tilde{\psi}^\dagger \rangle \approx \langle d^\dagger d \rangle = n_R = \int dx \langle \tilde{\psi}^\dagger(x) \tilde{\psi}(x) \rangle$. Following this crude approximation, the excitation Hamiltonian becomes $H_{ex} \approx g_l n_R \int dx (\psi_\downarrow(x) \psi_\uparrow(x) + h.c.)$. This has a form similar to the pairing terms in the BCS Hamiltonian. In particular, if it is combined with the BCS Hamil-

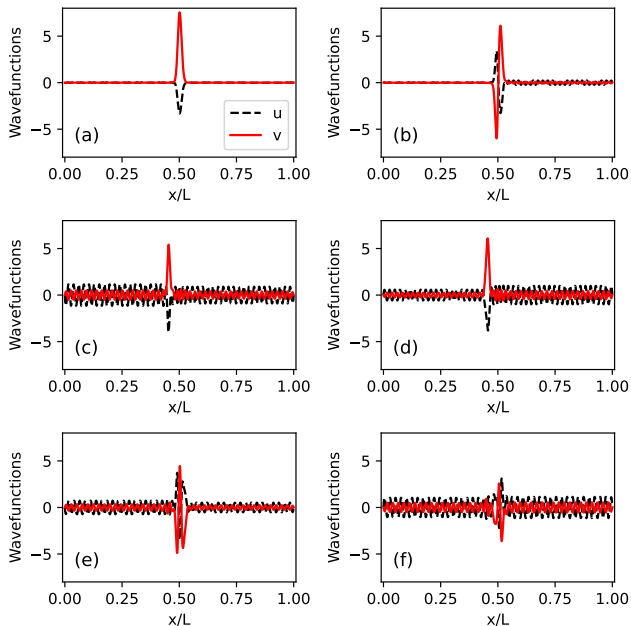


FIG. S7. Bound-state profiles of a Fermi superfluid in the BEC regime with $g = 3.8$ and $\mu = -0.06E_f$ with the Rb(62S) Rydberg potential. The magnitude of binding energies decreases monotonically following panels (a) to (f). Here (a) and (b) are the first two diatomic Rydberg-molecule states in the furthest well, (c) and (d) correspond to a triatomic molecule state in the secondary well, and (e) and (f) form another triatomic molecule state in the furthest well.

tonian, the resulting Hamiltonian leads to a suppressed pairing gap $\Delta' = \Delta - g_I n_R$, where Δ is the pairing gap in the absence of the Rydberg excitation. Therefore, exciting the Rydberg atoms directly from the Fermi superfluid instead of introducing different isotopes or species results in a suppression of the pairing gap and favors the formation of a diatomic Rydberg molecule with a fermion from a broken Cooper pair. Moreover, the Rydberg molecules are homonuclear if the Rydberg atoms are excitations of the Fermi superfluid. In contrast, the Rydberg molecules discussed in the main text are heteronuclear because the Rydberg atoms are different from the fermions in the superfluid.

VI. RYDBERG MOLECULES IN NONINTERACTING GASES

The energetically lowest six bound states obtained from the Schrödinger equation with the outer double-well approximation of the Rb(62S) Rydberg potential are provided in Fig. S8. Here, we follow the same scaling process (i.e., $\alpha = 0.5$) to place the furthest dip of the Rydberg potential at the middle of the box. We consider only one component of fermions here, as the other component will result in exactly the same results in a non-interacting system. By analyzing the number of nodes

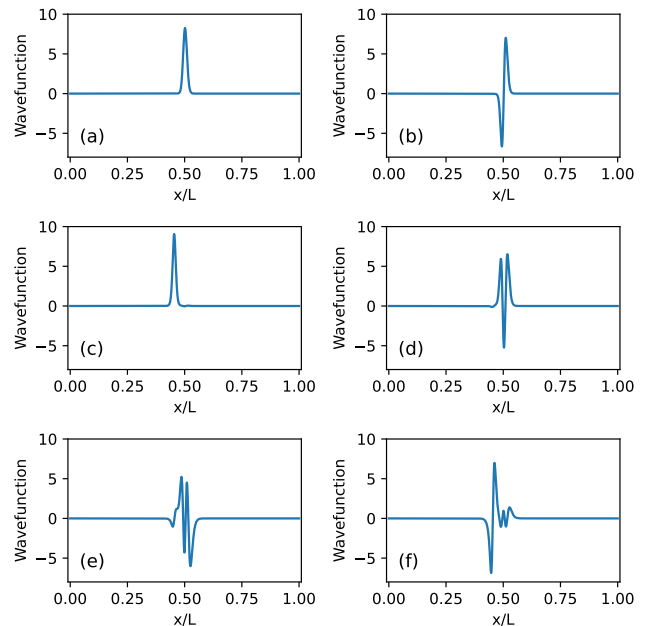


FIG. S8. Lowest six bound states of the Schrödinger equation within the two outer-well Rb(62S) Rydberg potential. The magnitude of binding energies decreases monotonically from (a) to (f). Panels (a), (b), (d), (e) show the first four bound states in the furthest well of the Rydberg potential. Panels (c) and (f) depict the lowest two bound states in the secondary well. The furthest Rydberg-potential well is located at $x = L/2$.

and the localization position of the wave functions, one can identify the series of the bound states localized in the furthest well of the Rydberg potential and the ones located in the secondary well. For example, panels (a), (b), (d), (e) of Fig. S8 showcase the first four bound states localized in the furthest dip, while panels (c) and (f) depict the two lowest bound states localized in the secondary well. Given the well-separated energies of the bound states, all bound states shown here correspond to diatomic Rydberg molecules between the Rydberg atom and a fermion. Their binding energies are extracted from the eigenvalues of the Schrödinger equation with the Rydberg potential. After proper normalization with respect to the values of E_f for the corresponding BCS and BEC cases, the binding energies are shown in Fig. 4 of the main text. We note in passing that triatomic Rydberg molecules binding a noninteracting spin- \uparrow fermion and a noninteracting spin- \downarrow fermion can also form. However, they will possess twice the binding energy of a corresponding diatomic Rydberg molecule. This is because for noninteracting fermions, each energy level can be occupied by one spin- \uparrow and one spin- \downarrow fermion since they do not feel the presence of each other. It should be emphasized that this binding process is different from the one of the triatomic Rydberg molecule encompassing a trapped Cooper pair, where pairing effects play a decisive role.